Original paper

Plimerite from Krásno near Horní Slavkov ore district, Czech Republic

Jiří SEJKORA[1*], Jakub PLÁŠIL[1, 2], Jan FILIP[3]

[1] *Department of Mineralogy and Petrology, National Museum, Václavské nám. 68, 115 79 Prague 1, Czech Republic; jiri_sejkora@nm.cz*
[2] *Department of Geological Sciences, Faculty of Science, Masaryk University, Kotlářská 2, 611 37 Brno, Czech Republic*
[3] *Centre for Nanomaterial Research and Department of Experimental Physics, Palacký University, Třída 17. listopadu 12, 779 00 Olomouc, Czech Republic*
[*] *Corresponding author*

The Zn-dominant analogue of rockbridgeite, recently described mineral plimerite, was found in samples from the Huber open pit, the Krásno near Horní Slavkov ore district, western Bohemia, Czech Republic. Plimerite occurs there in five morphologically different types, as black-green to black semi-spherical to spheroidal radiating aggregates (type 1), olive to grey-green aggregates formed by minute tabular crystals (type 2), dark green crystalline aggregates composed of tiny tabular crystals (type 3) and two types (4 and 5) of microscopic aggregates. All plimerite types were found in cavities of strongly altered original triplite accumulations; fluorapatite, isokite, kolbeckite, leucophosphite, beraunite, whitmoreite, kunatite and other rare phosphates were found in the association.

Detailed mineralogical data are given for plimerite type 1. The chemical analyses by EPMA (mean of nine points; wt. %) yielded Na_2O 0.48, CaO 0.51, FeO 4.87, BaO 0.04, MnO 0.93, ZnO 15.14, Fe_2O_3 32.47, Al_2O_3 3.04, SiO_2 0.05, As_2O_5 0.75, P_2O_5 32.56, H_2O_{calc} 5.11, total 95.94 wt. %. The resulting empirical formula on the basis of (As + P + Si) = 3 *apfu* is $(Zn_{1.20}Fe^{2+}_{0.44}Na_{0.10}Mn_{0.08}Ca_{0.06})_{\Sigma1.88}(Fe^{3+}_{2.62}Al_{0.38})_{\Sigma3.00}[(PO_4)_{2.95}(AsO_4)_{0.04}(SiO_4)_{0.01}]_{\Sigma3.00}(OH)_{3.65}$. Thermogravimetric data as same as infrared and Raman spectra indicate presence of weakly bonded molecular water in plimerite. Plimerite from Krásno is orthorhombic, space group *Bbmm*, with unit-cell parameters *a* 13.850(1), *b* 16.798(1), *c* 5.1581(3) Å and *V* 1200.1(2) Å³, *Z* = 4. The crystal structure was refined by the Rietveld method from the high-resolution synchrotron powder diffraction data to indices R_p 13.57%, R_{wp} 18.59% and R_{Bragg} 13.92% for 140 observed reflections. The refined crystal structure of plimerite from Krásno is related with those of rockbridgeite and of plimerite from Australia; the main differences are connected with the site-occupancies, derived from the site-symmetries and bond-valence parameters. Based on the crystal structure refinement, the formula for plimerite from Krásno is $(Zn_{1.20}Fe_{0.80})_{\Sigma2.00}Fe^{3+}_{3.32}(PO_4)_3(OH)_5 \cdot nH_2O$ (where n is probably < 1), Z = 4.

1. Introduction

Members of the frondelite–rockbridgeite series belong to frequent minerals observed as alteration products of primary phosphates in complex granite pegmatites, greisens, oxidation zones of the ore deposits and sedimentary phosphate deposits. Minor Zn contents in minerals of the frondelite–rockbridgeite series were reported from the Vinua do Castelo pegmatite, Maxedo, Portugal (5.20 wt. % ZnO – Lindberg and Frondel 1950), from granite pegmatites in Turkestan and the Kalbin Range, Central Asia (Ginzburg 1952) as well as from Sapucaia pegmatite, Minas Gerais, Brazil (Hirson 1965).

Birch (1990) described the first occurrence of rockbridgeite with a high zinc content (*c.* 30 % of Fe replaced by Zn) from the Kintore and Block 14 opencuts, Broken Hill, New South Wales (Australia). Sejkora et al. (2006b) reported high Zn contents (up to 19.19 wt. %

ZnO) in minerals of the rockbridgeite group from the Huber open pit in the Krásno ore district (Czech Republic). A characterization of this mineral was presented under the designation of an unnamed phase ”*UNK3*“. Finds of larger and better quality crystals of this mineral phase at the Block 14 Opencut (Broken Hill), provided suitable material for collection of the single-crystal X-ray data and a more complete characterization of this mineral. Consequently, the mineral was approved with the name plimerite by the IMA Commission on New Minerals, Nomenclature and Classification (Elliott et al. 2009). The study of Elliott et al. (2009) confirmed that Zn-rich rockbridgeite from the Reaphook Hill, Flinders Range, South Australia (Johnson 1978) is also plimerite. The aim of this paper is to describe of plimerite from Krásno and to clarify the role of Zn and possible content of molecular water in this mineral phase.

2. Occurrence and sample description

The studied plimerite samples were found in ~1985–1995 by mineral collector Ctibor Süsser, who donated several specimens to the National Museum, Prague. They have been found at supergene altered phosphate accumulations in the abandoned Huber open pit, Krásno near Horní Slavkov in the Czech Republic (Sejkora et al. 2006a–c). The Huber open pit, exposing the apical, greisenized part of autometamorphosed Li-mica–topaz granite cupola, was mined for Sn and W ores in the past. Detailed descriptions of geology and mineralogy of the whole Sn–W ore district Krásno near Horní Slavkov were published by Beran and Sejkora (2006) and Sejkora et al. (2006a, c).

At the Huber open pit, plimerite was found in cavities of strongly altered original triplite accumulations in the following five morphological types (Sejkora et al. 2006b).

Plimerite type 1 forms abundant semi-spherical to spheroidal radiating aggregates up to 1.5 mm in size, locally clustering to aggregates up to 2 mm (Fig. 1) in association with light yellow-grey imperfect crystals of young fluorapatite. They occur in cavities (1–2 mm in diameter) of triplite aggregates, altered to compact red-brown fluorapatite and isokite. This material is accompanied by coarse-grained white quartz containing grains (up to 2 cm) of dark green fluorapatite. The plimerite type 1 aggregates are black-green to black with a green hue, vitreous on fracture, with a greasy lustre. Its minute splinters are transparent, bright green, and have a light grey-green streak. The surface of the aggregates consists of intergrown tabular crystals 20–40 μm long, oriented perpendicular to the surface of the spherical aggregates (Fig. 2).

Fig. 2 Tabular crystals of plimerite (type 1) on the surface of plimerite spherical aggregates. Huber open pit, Krásno, width of photo 75 μm. Jeol JSM-6380, SEM photo by J. Sejkora and J. Plášil.

Plimerite type 2 has been found in strongly altered aggregate of pinkish and white fluorapatite, 7 by 10 cm in size. Plimerite forms soft and crumbly olive to grey-green aggregates (Fig. 3) up to 2 cm across, deposited in irregular cavities in fluorapatite 5 by 6 cm in size. These aggregates consist of minute well-formed crystals (Fig. 4) up to 100 μm long in association with frequent white to light green fluorapatite and less abundant greyish white kolbeckite aggregates. Individual tabular crystals of plimerite are green to black with a green hue and have a vitreous lustre.

Plimerite type 3 occurs in weathered vugs (2 by 3 cm in size) in fluorapatite/isokite accumulations with triplite relics. It forms dark green crystalline aggregates 0.5–1 mm in diameter, composed of tabular crystals up to 0.1 mm long (Fig. 5). Plimerite aggregates with a strong vitreous lustre, showing occasional rhombic cross-

Fig. 1 Black-green spherical aggregates of plimerite (type 1) with light brown fluorapatite. Huber open pit, Krásno, width of the area shown 4.5 mm. Nikon SMZ1500 microphoto by J. Sejkora.

Fig. 3 Olive-green crystalline aggregates of plimerite (type 2) with light brown fluorapatite. Huber open pit, Krásno, width of the area shown 3.5 mm. Nikon SMZ1500, photomicrograph by J. Sejkora.
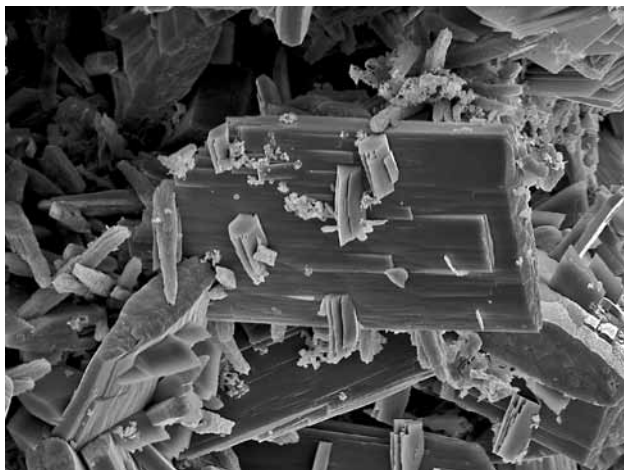
Fig. 4 Tabular crystals of plimerite (type 2). Huber open pit, Krásno, width of photo 80 μm. Jeol JSM-6380, SEM photo by J. Sejkora and J. Plášil.
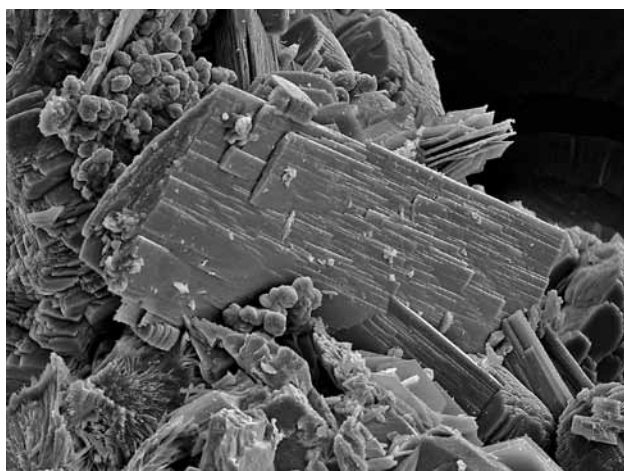
Fig. 5 Tabular crystals of plimerite (type 3). Huber open pit, Krásno, width of photo 110 μm. Jeol JSM-6380, SEM photo by J. Sejkora and J. Plášil.
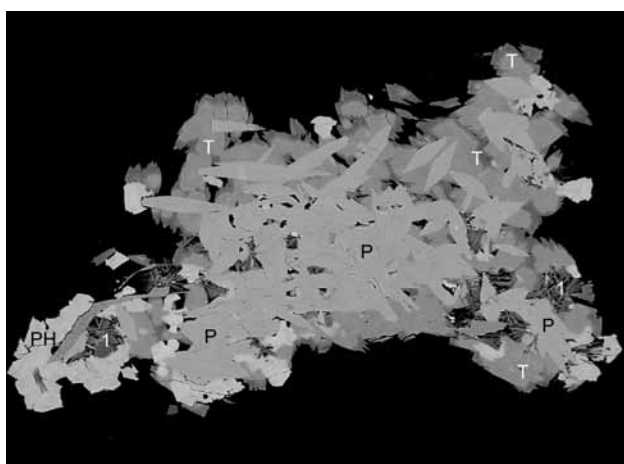
Fig. 6 Aggregate of tabular crystals of plimerite (type 3) (in places with rhombic section – P), overgrown by zoned aggregates of turquoise-group mineral (T), tabular crystals of *UNK1* (1) and pharmacosiderite (PH) crystals. Huber open pit, Krásno, width of photo 500 μm. Cameca SX100, BSE photo by J. Sejkora and R. Škoda.

sections (Fig. 6), are usually overgrown by zoned aggregates of minerals of turquoise-group, including *UNK10* (Sejkora et al. 2006b), pharmacosiderite, *UNK1* (Sejkora et al. 2006b), rare kolbeckite and Cl-rich fluorapatite. Kunatite (Mills et al. 2008), leucophosphite, whitmoreite, earlshanonnite, *UNK7* and *UNK8* (Sejkora et al. 2006b) were also observed in this association.

Plimerite type 4 forms microscopic (up to 30 μm) irregular inclusions (Fig. 7) in acicular to fibrous Zn- and Al-rich beraunite associated with fluorapatite and irregular crystals and aggregates of K-poor leucophosphite (Sejkora et al. 2006c).

Plimerite type 5 was found as irregular aggregates up to 100 μm in size (Fig. 8), which (with whitmoreite)
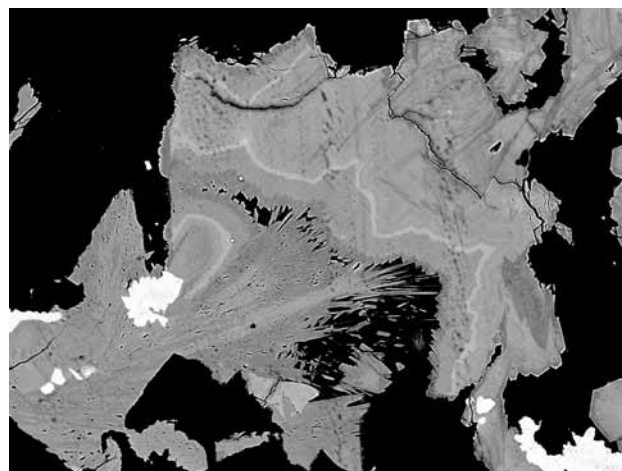
Fig. 7 White grains of plimerite (type 4) in zoned crystalline aggregates of K-deficient leucophosphite and fibrous Zn- and Al-rich beraunite. Huber open pit, Krásno, width of photo 300 μm. Cameca SX100, BSE photo by J. Sejkora and R. Škoda.
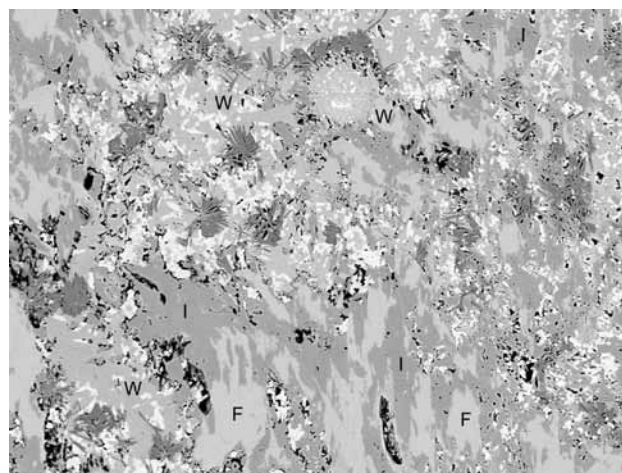
Fig. 8 The oldest mineral fluorapatite (marked F) is replaced by isokite (I); aggregates of these two minerals are in turn replaced by whitmoreite (W) and abundant grains of very light plimerite (type 5). All these minerals are replaced by the youngest dark tabular crystals of *UNK1*. Huber open pit, Krásno, width of photo 600 μm. Cameca SX100, BSE photo by J. Sejkora and R. Škoda.

Tab. 1 Chemical composition of plimerite type 1 from Krásno, compared with published data

	Krásno type 1 (this paper)										Elliott et al. (2009)			
	mean	1	2	3	4	5	6	7	8	9	1*	2*	3*	4*
Na_2O	0.48	0.43	0.49	0.52	0.55	0.47	0.44	0.47	0.45	0.48	0.00	0.00	0.00	0.00
CaO	0.51	0.46	0.53	0.50	0.56	0.55	0.56	0.30	0.48	0.61	0.17	0.80	0.14	1.41
FeO	4.87	6.03	5.38	5.82	4.03	4.15	4.09	5.33	6.16	2.80	3.30	0.20	4.87	4.64
BaO	0.04	0.20	0.00	0.09	0.03	0.00	0.04	0.00	0.00	0.00	0.00	0.00	0.00	0.00
MgO	0.00	0.00	0.00	0.00	0.00	0.00	0.00	0.00	0.00	0.00	0.00	0.11	0.00	0.84
PbO	0.00	0.00	0.00	0.00	0.00	0.00	0.00	0.00	0.00	0.00	0.36	0.20	0.37	0.03
CuO	0.00	0.00	0.00	0.00	0.00	0.00	0.00	0.00	0.00	0.00	0.00	0.00	0.24	0.00
MnO	0.93	0.96	1.10	1.00	0.94	0.86	1.01	0.63	0.85	1.06	0.02	0.36	0.04	0.56
ZnO	15.14	14.79	14.40	14.87	14.90	15.10	15.63	15.51	14.09	16.98	20.17	18.52	14.43	18.38
Fe_2O_3	32.47	32.49	32.84	32.87	33.27	32.47	33.07	31.03	31.15	33.02	29.46	35.30	35.98	32.50
Al_2O_3	3.04	3.59	2.69	3.26	2.93	3.16	2.88	3.45	3.01	2.37	4.48	1.89	0.93	1.48
SiO_2	0.05	0.13	0.07	0.26	0.00	0.00	0.00	0.00	0.00	0.00	0.00	0.00	0.00	0.00
As_2O_5	0.75	0.85	0.80	0.91	0.73	1.01	0.72	0.68	0.52	0.57	0.09	0.05	0.23	0.04
P_2O_5	32.56	33.20	32.36	32.89	33.20	32.64	32.96	31.96	31.55	32.30	32.37	33.98	33.13	30.92
H_2O	5.11	5.30	5.12	5.29	4.89	4.91	5.06	5.16	5.16	5.07	5.38	4.56	4.55	6.20
Total	95.94	98.42	95.78	98.26	96.03	95.33	96.46	94.52	93.40	95.26	95.80	95.98	94.90	97.00
Na^+	0.099	0.086	0.101	0.105	0.112	0.097	0.091	0.099	0.096	0.102	0.000	0.000	0.000	0.000
Ca^{2+}	0.058	0.051	0.061	0.056	0.063	0.063	0.064	0.035	0.058	0.071	0.020	0.089	0.016	0.173
Fe^{2+}	0.436	0.528	0.484	0.511	0.355	0.370	0.363	0.488	0.572	0.254	0.301	0.018	0.434	0.444
Ba^{2+}	0.002	0.008	0.000	0.004	0.001	0.000	0.002	0.000	0.000	0.000	0.000	0.000	0.000	0.000
Mg^{2+}	0.000	0.000	0.000	0.000	0.000	0.000	0.000	0.000	0.000	0.000	0.000	0.017	0.000	0.143
Pb^{2+}	0.000	0.000	0.000	0.000	0.000	0.000	0.000	0.000	0.000	0.000	0.011	0.006	0.011	0.001
Cu^{2+}	0.000	0.000	0.000	0.000	0.000	0.000	0.000	0.000	0.000	0.000	0.000	0.000	0.019	0.000
Mn^{2+}	0.085	0.085	0.100	0.089	0.083	0.078	0.091	0.058	0.080	0.097	0.002	0.032	0.004	0.054
Zn^{2+}	1.197	1.142	1.144	1.152	1.158	1.188	1.224	1.253	1.157	1.361	1.628	1.425	1.135	1.554
$\Sigma M2$	1.877	1.900	1.891	1.917	1.774	1.796	1.835	1.934	1.963	1.886	1.961	1.586	1.618	2.370
Fe^{3+}	2.617	2.557	2.659	2.597	2.636	2.603	2.641	2.555	2.606	2.697	2.423	2.768	2.883	2.800
Al^{3+}	0.383	0.443	0.341	0.403	0.364	0.397	0.359	0.445	0.394	0.303	0.577	0.232	0.117	0.200
$\Sigma M1+M3$	3.000	3.000	3.000	3.000	3.000	3.000	3.000	3.000	3.000	3.000	3.000	3.000	3.000	3.000
Si^{4+}	0.005	0.014	0.007	0.027	0.000	0.000	0.000	0.000	0.000	0.000	0.000	0.000	0.000	0.000
As^{5+}	0.042	0.046	0.045	0.050	0.040	0.056	0.040	0.039	0.030	0.032	0.005	0.003	0.013	0.002
P^{5+}	2.952	2.940	2.948	2.923	2.960	2.944	2.960	2.961	2.970	2.968	2.995	2.997	2.987	2.998
Σ	3.000	3.000	3.000	3.000	3.000	3.000	3.000	3.000	3.000	3.000	3.000	3.000	3.000	3.000
OH	3.651	3.698	3.674	3.704	3.435	3.489	3.581	3.766	3.827	3.671	3.922	3.169	3.232	4.736

Empirical formulae were calculated on the basis of (P + As + Si) = 3; H_2O contents were obtained from the charge balance; FeO/Fe_2O_3 were estimated from the occupancy $M1 + M3$ by Fe^{3+} and $M2$ only by Fe^{2+}.
1* Broken Hill (G32005), 2* Broken Hill (G32405), 3* Broken Hill (G32401), 4* Reaphook Hill, all data of Elliott et al. (2009)

replace older aggregates of isokite and fluorapatite. Plimerite aggregates, together with other older phosphates, are replaced by the youngest tabular crystals of *UNK1* (Sejkora et al. 2006b).

Types 1–3 of plimerite from Krásno were identified by conventional powder XRD (Sejkora et al. 2006b) and EPMA; types 4 and 5 of plimerite, with regard to their size are characterised only by EPMA. Plimerite type 1 was selected for a detailed mineralogical study (crystallographic data, thermal analysis, Raman and infrared spectroscopy).

3. Chemical analyses and thermogravimetric data

3.1. Experimental

Plimerite samples from Krásno were analysed with a Cameca SX-100 electron microprobe (Joint Laboratory of Electron Microscopy and Microanalysis of Masaryk University and Czech Geological Survey, Brno) operating in the wavelength-dispersion mode with an accelerating voltage of 15 kV, a specimen current of 10 nA, and a

beam diameter of 5–10 μm. In order to minimize peak overlaps, the following analytic lines and crystals were selected: K_α lines: F (PC1, fluorapatite/topaz), Mg (TAP, forsterite), Na (TAP, albite), Al (TAP, sanidine), As (TAP, InAs), Si (TAP, sanidine), Cu (TAP, dioptase), K (PET, sanidine), P (PET, fluorapatite) Ca (PET, andradite), S (PET, barite), Ti (PET, TiO), Cl (PET, vanadinite), Fe (LIF, andradite), Mn (LIF, rhodonite), Zn (LIF, ZnO); L_α lines: Sr (PET, SrSO$_4$); L_β lines: Ba (PET, benitoite); M_α lines: Pb (PET, vanadinite). Peak counting times were 20 s for the main elements and 60 s for minor elements; background was acquired for ½ of the peak time. The raw intensities were converted to the concentrations using automatic *PAP* (Pouchou and Pichoir 1985) matrix correction software package. Contents of Cl, Cu, F, K, Mg, S and Sr were sought for but were below the detection limit (*c.* 0.01–0.03 wt. %).

Thermogravimetric curve of plimerite (type 1) from Krásno was recorded on TG 750 Stanton Redcroft Thermobalance. The operating conditions were: weight = 2.358 mg, heating rate = 10 °C/min, dynamic air atmosphere = 10 ml/min, and temperature range = 20–920 °C.

3.2. Results

The quantitative chemical analyses of five morphologically different types of plimerite from Krásno are given in Tabs 1 and 2, together with data published by Elliott et al. (2009). All chemical analyses were recalculated on the basis of (P + As + Si) = 3 *apfu*. On the basis of new

structural investigation and reinterpretation of structural data published by Elliott et al. (2009), three different cation positions (*M1-M3*) exist in the crystal structure of plimerite. The *M1*-position (1 *apfu*) is occupied by Fe^{3+} and at the *M3*-position (2 *apfu*) Fe^{3+} and Al are located. The *M2*-position (2 *apfu*) contains predominately Zn and other M^{1+}, M^{2+} cations, as well as Fe. We assume that majority of Fe in *M2*-position is divalent. Elliott et al. (2009) assumed, on the basis of chemical and structure analyses, significant content of Fe^{3+} (0.42 *apfu*) in addition to Fe^{2+} (0.38 *apfu*) in this position. A recalculation of the chemical analysis by Elliott et al. (2009) yields 0.43 *apfu* Fe^{2+} at *M2*-position (Tab. 1) – i. e., 13 % of total Fe, a value near published data (Elliot et al. 2009) from the Mössbauer spectroscopy (11 % of Fe occurs as Fe^{2+}).

Dominant Zn contents (0.87–1.49 *apfu*) in *M2*-position are characteristic of plimerite from Krásno (Fig. 9). These zinc contents correspond to data published for plimerite from Australian occurrences (Elliott et al. 2009). The highest Zn content was determined in plimerite types 4 and 5 (1.38–1.49 *apfu*), the lowest in plimerite type 3 (0.87–0.99 *apfu*). In addition to minor contents of Ba and Pb (up to 0.01 *apfu*) in the *M2*-position, there are contents of Ca, Na and Mn (0.07–0.12 *apfu*) and Fe^{2+} up to 0.73 *apfu*. The total occupancy of the *M2*-position, 1.61–1.96 *apfu* is near the theoretical 2 *apfu*.

The *M3*-position of plimerite from Krásno (Fig. 10) contains minor Ti^{4+} (up to 0.06 *apfu*) and Al in the range of 0.30–0.60 *apfu,* besides dominant Fe^{3+}. Similar elevated Al contents have been found in one plimerite
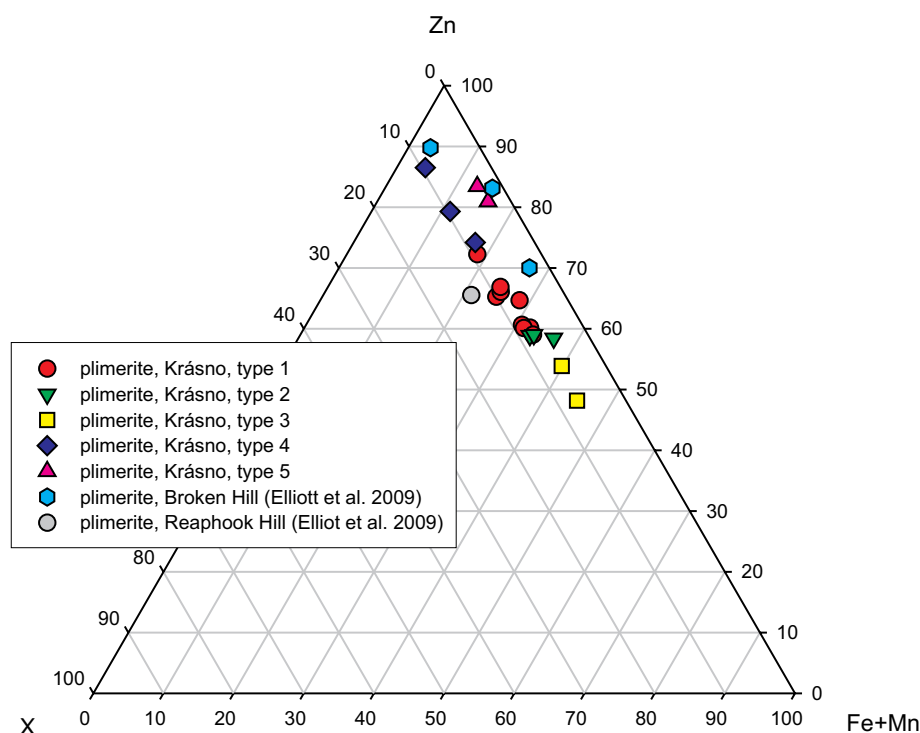
Fig. 9 Ternary plot of X – Zn – (Fe + Mn) of *M2*-site occupancy (atomic ratios) for plimerite. X = Na + Ca + Ba + Mg + Pb + Cu in *M2*-site
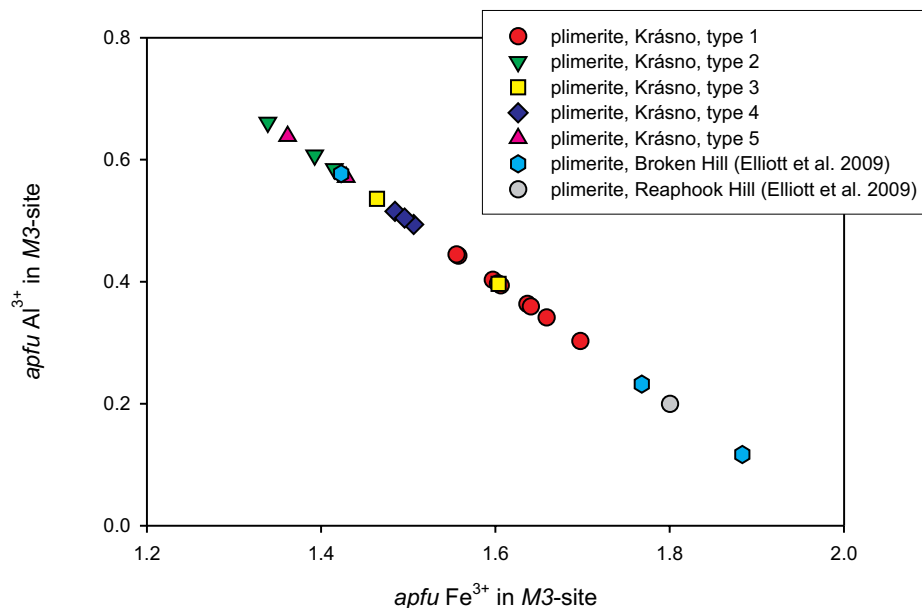
Fig. 10 Plot of Fe^{3+} – Al^{3+} occupancy in *M3*-site of plimerite.
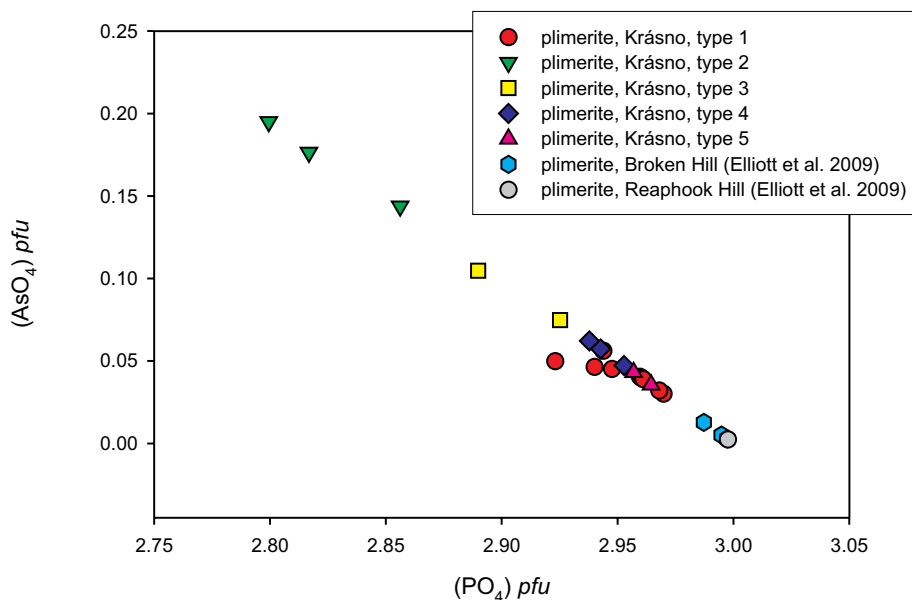
Fig. 11 Plot of (PO_4) – (AsO_4) *pfu* in tetrahedral site of plimerite.
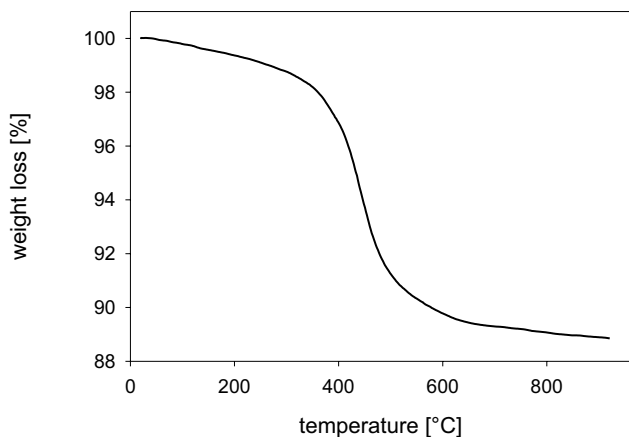
Fig. 12 Thermogravimetric curve of plimerite from Krásno.

sample from Broken Hill (Elliott et al. 2009) and in minerals of the frondelite–rockbridgeite series from Krásno (Sejkora et al. 2006c). The tetrahedral sites of plimerite from Krásno host, besides dominant P, also significant contents of As (0.03–0.10 *apfu*, and in type 2 plimerite of 0.14–0.19 *apfu*) (Fig. 11). Plimerite from Australian occurrences contains only max. 0.01 *apfu* As (Elliott et al. 2009). Some plimerite samples from Krásno (type 1) also contain minor Si (up to 0.03 *apfu*).

The presence of Zn and other M^{1+} and M^{2+} atoms in the *M2*-position results in decrease of number of OH groups from five (given for the frondelite–rockbridgeite series) to four in the case of plimerite (the range calculated on the basis of charge balance is 3.24–3.85 *pfu*). None of the studied samples shows substitution of OH by Cl or

Tab. 2 Chemical composition of plimerite types 2–5 from Krásno

	type 2				type 3			type 4				type 5		
	mean	1	2	3	mean	1	2	mean	1	2	3	mean	1	2
Na_2O	0.43	0.53	0.34	0.43	0.39	0.37	0.41	0.51	0.50	0.46	0.56	0.06	0.08	0.04
CaO	0.26	0.25	0.14	0.38	0.31	0.29	0.32	0.47	0.49	0.52	0.41	0.36	0.36	0.36
FeO	6.87	6.54	7.30	6.75	7.75	7.48	8.02	1.32	1.31	0.02	2.61	2.22	1.86	2.59
BaO	0.11	0.15	0.18	0.00	0.00	0.00	0.00	0.09	0.12	0.16	0.00	0.08	0.02	0.14
PbO	0.18	0.27	0.00	0.26	0.09	0.10	0.09	0.03	0.00	0.10	0.00	0.00	0.00	0.00
MnO	0.10	0.12	0.14	0.03	0.61	0.45	0.77	0.90	0.86	0.73	1.11	0.49	0.52	0.47
ZnO	13.57	13.59	13.50	13.63	11.45	12.13	10.77	18.24	17.43	19.19	18.10	17.49	17.42	17.57
Fe_2O_3	28.58	29.01	27.87	28.86	30.15	29.37	30.92	30.63	31.18	30.75	29.95	29.85	30.49	29.21
Al_2O_3	4.75	4.72	5.05	4.47	3.60	4.13	3.07	4.04	4.01	4.17	3.93	4.85	4.62	5.08
SiO_2	0.04	0.06	0.05	0.00	0.02	0.05	0.00	0.00	0.00	0.00	0.00	0.00	0.00	0.00
As_2O_5	2.98	3.09	3.36	2.48	1.56	1.82	1.31	1.00	1.14	0.86	1.01	0.71	0.65	0.77
P_2O_5	30.21	30.48	29.76	30.39	31.27	30.97	31.58	32.80	33.19	33.26	31.93	33.08	33.40	32.75
TiO_2	0.09	0.11	0.10	0.05	0.52	0.34	0.70	0.65	0.68	0.74	0.52	0.26	0.29	0.22
H_2O	4.99	4.95	5.03	4.99	4.90	4.92	4.90	4.99	4.80	4.85	5.30	4.73	4.62	4.83
Total	93.13	93.87	92.81	92.71	92.62	92.40	92.85	95.66	95.70	95.83	95.44	94.18	94.32	94.03
Na^+	0.093	0.112	0.074	0.093	0.082	0.078	0.086	0.104	0.101	0.094	0.118	0.013	0.017	0.009
Ca^{2+}	0.031	0.030	0.016	0.046	0.036	0.035	0.037	0.054	0.055	0.059	0.048	0.041	0.040	0.041
Fe^{2+}	0.634	0.597	0.679	0.626	0.712	0.689	0.734	0.117	0.115	0.002	0.238	0.196	0.163	0.231
Ba^{2+}	0.005	0.006	0.008	0.000	0.000	0.000	0.000	0.004	0.005	0.007	0.000	0.003	0.001	0.006
Pb^{2+}	0.005	0.008	0.000	0.008	0.003	0.003	0.003	0.001	0.000	0.003	0.000	0.000	0.000	0.000
Mn^{2+}	0.009	0.011	0.014	0.003	0.057	0.042	0.072	0.081	0.076	0.065	0.102	0.044	0.046	0.043
Zn^{2+}	1.107	1.096	1.108	1.117	0.928	0.987	0.870	1.428	1.345	1.486	1.455	1.366	1.348	1.383
$\Sigma M2$	1.883	1.860	1.898	1.893	1.818	1.834	1.802	1.789	1.698	1.715	1.961	1.663	1.615	1.713
Fe^{3+}	2.375	2.384	2.331	2.411	2.491	2.436	2.546	2.444	2.453	2.426	2.453	2.375	2.406	2.344
Al^{3+}	0.618	0.607	0.661	0.585	0.466	0.536	0.396	0.505	0.494	0.515	0.504	0.605	0.571	0.638
Ti^{4+}	0.007	0.009	0.008	0.004	0.043	0.028	0.058	0.051	0.053	0.058	0.042	0.020	0.023	0.017
$\Sigma M1+M3$	3.000	3.000	3.000	3.000	3.000	3.000	3.000	3.000	3.000	3.000	3.000	3.000	3.000	3.000
Si^{4+}	0.004	0.007	0.006	0.000	0.003	0.005	0.000	0.000	0.000	0.000	0.000	0.000	0.000	0.000
As^{5+}	0.172	0.176	0.195	0.144	0.090	0.105	0.075	0.056	0.062	0.047	0.057	0.039	0.036	0.043
P^{5+}	2.824	2.817	2.799	2.856	2.908	2.890	2.925	2.944	2.938	2.953	2.943	2.961	2.964	2.957
Σ	3.000	3.000	3.000	3.000	3.000	3.000	3.000	3.000	3.000	3.000	3.000	3.000	3.000	3.000
OH	3.676	3.605	3.729	3.696	3.590	3.617	3.577	3.530	3.348	3.392	3.848	3.336	3.231	3.436

Empirical formulae were calculated on the basis (P + As + Si) = 3; H_2O contents were obtained from the charge balance; FeO/Fe_2O_3 were estimated from the occupancy $M1 + M3$ by Fe^{3+} and $M2$ only by Fe^{2+}.

F. A similar situation was described for minerals of the frondelite–rockbridgeite series from Krásno by Sejkora et al. (2006c).

The empirical formula of type 1 plimerite (mean of 9 analyses), which was used for a detailed mineralogical study can be expressed based on (As + P + Si) = 3 *apfu* as $(Zn_{1.20}Fe^{2+}_{0.44}Na_{0.10}Mn_{0.08}Ca_{0.06})_{\Sigma 1.88}$ $(Fe^{3+}_{2.62}Al_{0.38})_{\Sigma 3.00}$ $[(PO_4)_{2.95}(AsO_4)_{0.04}(SiO_4)_{0.01}]_{\Sigma 3.00}(OH)_{3.65}$.

Other empirical formulae corresponding to individual spot analyses and means for all plimerite types from Krásno are presented in Tabs 1 and 2.

Plimerite thermally decomposes in three steps (Fig. 12). Approximately one weakly bonded water molecule is gradually liberated first at 20–370 °C (2.5 wt. %). In the range of 370–470 °C is released 5.5 wt. % of water bound as OH groups. This closely corresponds to the value 5.11 wt. % calculated from the EPMA data (Tab. 1). The weight loss of 3.0 wt. % in the range 470–920 °C is probably caused by decomposition reaction of an anhydrous phase formed in the previous steps – e.g. release of part of O_2, ZnO and probably a minor As_2O_3. The presence of weakly bonded molecular water in plimerite was confirmed by results of Raman and infrared spectroscopy (see below) and it is also may be indicated by lower totals of EPMA data (Tabs 1 and 2).

4. Raman and infrared spectroscopy

4.1. Experimental

The Raman spectrum of plimerite sample from Krásno, in the range 110–4000 cm^{-1}, was collected with a Labram HR dispersive Raman spectrometer (Jobin Yvon) with a confocal Olympus microscope. The Raman signal was excited by a 532.2 nm laser and detected with a multi-channel air-cooled CCD camera. The laser power was restricted to 5 mW in order to limit a possible thermal damage of the sample.

The infrared spectrum of the sample, mixed with KBr powder, was recorded by the microdiffuse reflectance method (DRIFTS) on a Nicolet Magna 760 FTIR spectrometer (range 600–4000 cm^{-1}, resolution 4 cm^{-1}, 128 scans, Happ–Genzel apodization), equipped with a Spectra Tech InspectIR micro-FTIR accessory. Both spectral data sets were processed using Omnic Spectral tool software.

4.2. Results

Both the Raman and infrared spectra of plimerite from Krásno exhibit similar characteristics as those published by Elliott et al. (2009) for plimerite from Australia.

A dominant feature of the vibrational spectra of plimerite from Krásno (Figs 13–14) is a PO_4 stretching region. By the analysis of the spectra a suite of overlapping bands adhering to ν_1 and ν_3 stretching modes of phosphate tetrahedra was obtained (Tab. 3, Fig. 15). As clearly visible from the Raman spectrum of plimerite, ν_3 stretching vibration is activated due to the decrease in the molecular T_d symmetry. By the inspection of Raman and infrared intensities we should conclude that the shift between two stretching modes is in case of plimerite small. According to decomposition of the Raman spectrum, up to 8 reliable bands can be observed. This value is consistent with possible split of ν_3 (F_2) stretching vibration (2 symmetrically non-equivalent P atoms in the asymmetric unit) and its activation in the Raman spectrum.

Bending modes of phosphate tetrahedra ν_4 (F_2) and ν_2 (E) occur between ~650 and ~400 cm^{-1} (Tab. 3), overlapping with stretching/bending vibrations of AlO_6 octahedra. The bands below 400 cm^{-1} are difficult to assign; overlapping vibrations of XO_6 octahedra (X = Fe and Zn), lattice modes and soft phonons should occur there.

The second dominant feature in the vibrational spectra of plimerite from Krásno is a region of OH stretching vibrations. Inspecting Fig. 14, the broad, relatively non-differentiated band, with a maximum at 3228 cm^{-1}, is clearly visible. This band should be assigned to the ν_1 and ν_3 OH stretching vibrations of the molecular H_2O. It is relatively weakly bonded, as suggests a band-shape in the Raman spectrum and a weak, quite symmetric band at ~1600 cm^{-1}, adhering to ν_2 (δ) H_2O (both infrared and Raman). The sharp band occurring in Raman and infrared spectra at ~3590 cm^{-1} corresponds to the stretching vibrations of OH$^-$ groups in the crystal structure of plimerite.
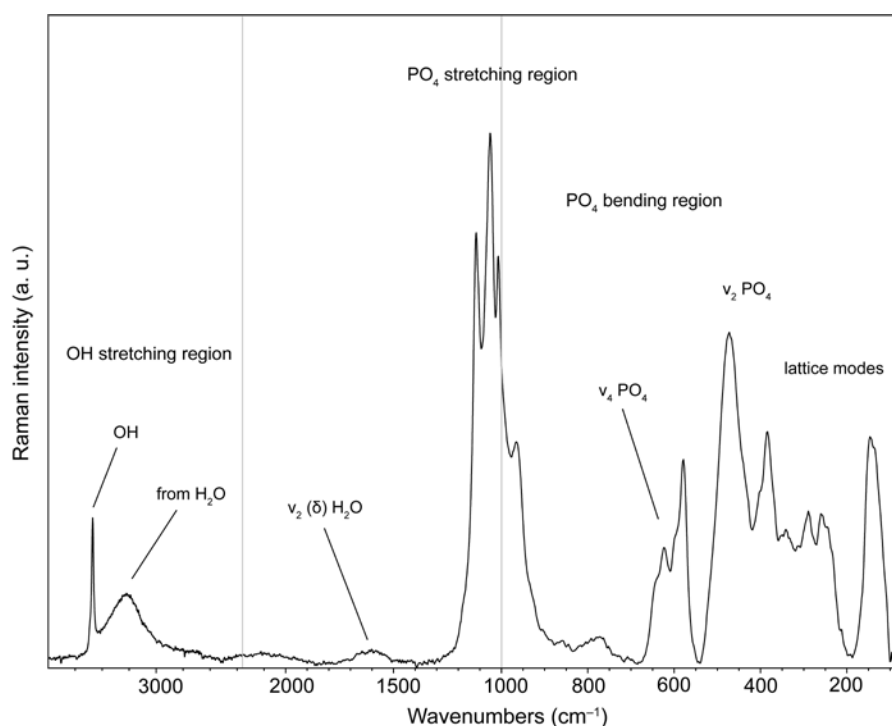
Fig. 13 Raman spectrum of plimerite sample from Krásno. Tentative assignments of the bands are displayed for clarity.
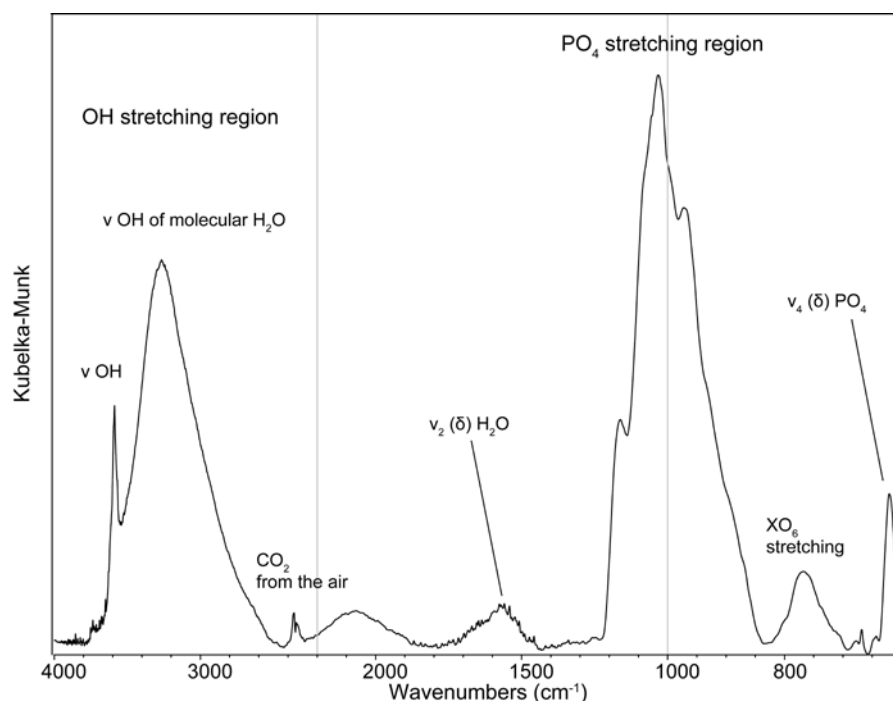
Fig. 14 Infrared spectrum of plimerite sample from Krásno. Tentative assignments of the bands are displayed for clarity.
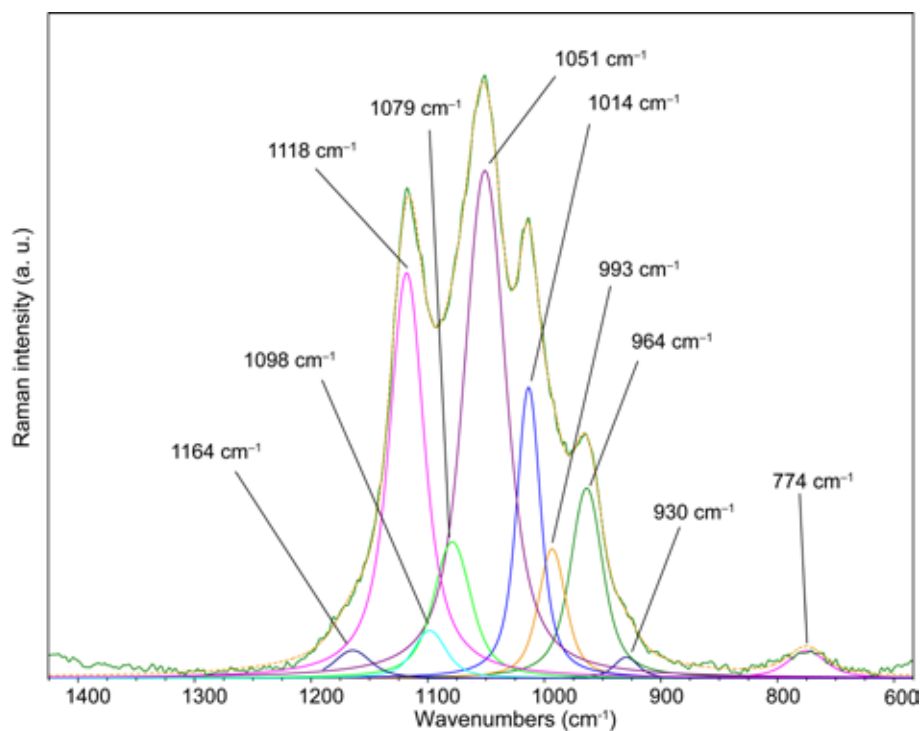
Fig. 15 Decomposition of the Raman spectrum of plimerite from Krásno in the region of the stretching vibrations of phosphate tetrahedra. The band shape was described by Gauss-Lorentzian profile function, the position, height and *FWHM* parameters were refined until the r^2 correlation parameter was better than 0.95.

5. Crystal structure refinement

5.1. Experimental

Preliminary X-ray powder diffraction patterns of plimerite sample from Krásno were collected on the PANalytical X'Pert Pro powder diffractometer with X'Celerator solid-state detector using CoK_α radiation.

The second data set used for crystal structure refinement was collected at the bending magnet of the PDIFF beamline, ANKA synchrotron source (KIT, Karlsruhe, Germany). A monochromatic radiation of the energy 14.99 keV (0.82694 Å) was selected from the white beam by the double crystal Si(111) monochromator and focused with the vertically and horizontally focusing mirror system. The wavelength and the zero angle of the

Tab. 3 Raman and infrared wavenumbers with a tentative assignment

Raman position (cm⁻¹)/rel. intensity	Infrared position (cm⁻¹)/rel. intensity	Assignment
3588/27	3589/ms	ν OH stretching of OH⁻ and weakly bonded molecular H_2O
3419/15		
3250/11	3228/s*	
1596/4	1600/sh	ν_2 (δ) H_2O
	1570/w	
1164/9	1162/w	ν_3 and ν_1 PO_4 stretching region
1118/98		
1098/32	1083/sh	
1079/57	1056/sh	
1051/100	1031/vs	
1014/83		
993/26		
964/46	973/s	
930/5	932/sh	
775/6	769/mw	Al–O stretch
	679/vw	
	668/w	
	662/w	ν_4 (δ) PO_4
644/14	648/w	
622/21	621/ms	
598/22		
578/38		ν_2 (δ) PO_4
474/68		
434/15		
408/13		
383/40		overlapping modes of Fe/ZnO₆ octahedra and lattice modes
339/21		
292/24		
249/27		
149/36		
128/35		

diffractometer were determined with silicon powder (NIST standard reference material 640). Plimerite sample was loaded into a 0.3 mm glass capillary which was rotated around its axis during data collection. The intensity of the incident beam was monitored during the data collection by an ion chamber and the measured intensities of the diffracted beam were corrected for the decay and fluctuations of the primary beam. The XRD patterns were collected at room temperature with the scintillation counter and Ge(111) analyser, over an angular range of 4–35 °2θ, with the step of 0.005 °2θ and counting time of 2 s per point. JANA2006 software (Petříček et al. 2006) was utilized for the Rietveld refinement of the plimerite crystal structure.

The crystal data for the sample G32401 (Elliot et al. 2009) were used as an initial structural model in the refinement. By analogy to the work of Elliot et al. (2009), the non-

Plimerite, Krásno (CZ)
Synchrotron powder diffraction (0.82694 Å)
a = 13.8506(10), *b* = 16.7981(10), *c* = 5.1581(3) Å, *V* = 1200.1(2) Å³
R_p = 0.136, R_{wp} = 0.186, R_{Bragg} = 0.139, R_F = 0.073, GOF = 2.11
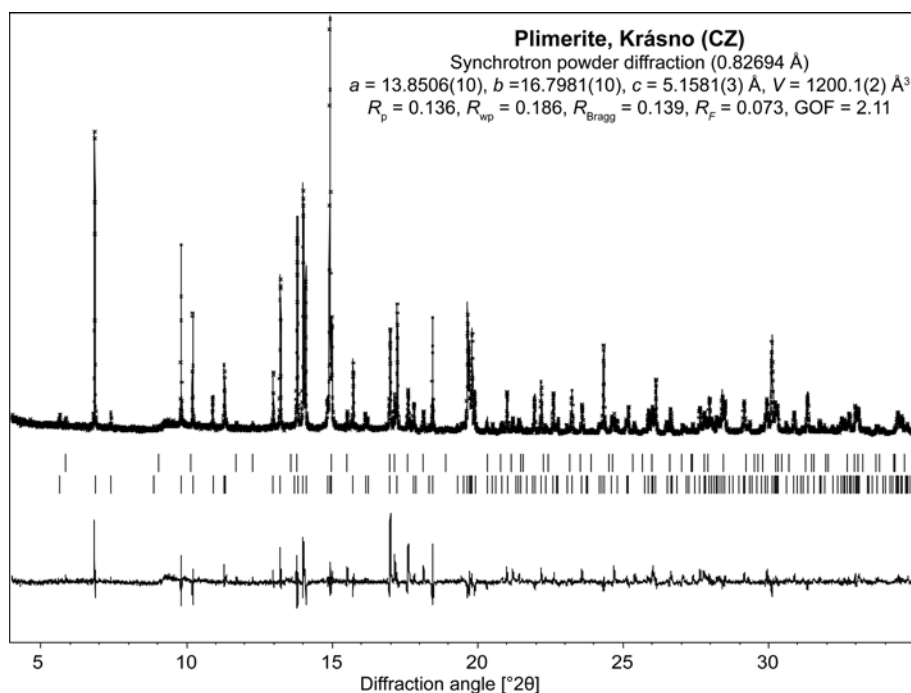
Fig. 16 Final Rietveld plot for refinement of the crystal structure of plimerite showing observed (asterisks), calculated (solid line) and difference (solid line at the bottom of the picture) profiles. Vertical bars correspond to the Bragg positions of the diffractions of fluorapatite (upper) and plimerite (lower).

Tab. 4 Data collection, crystal data and Rietveld refinement of plimerite from Krásno

Data collection	
Source	ANKA synchrotron, 1.5T bending magnet
Energy (wavelength)	14.99 keV (0.82694 Å)
Monochromators	Primary double crystal Si(111) and analyzer Ge(111)
Diffractometer, detector	Kappa diffractometer, scintillation counter
Sample	Powder, 0.3 mm capillary
Range/ step size/ counting time	4–35 º2θ/ 0.005 º2θ/ 2 s per step
Crystal data	
Structural formula	$Zn_{1.20}Fe_{4.13}(PO_4)_3(OH)_5$
Space group	*Bbmm* (# 63)
Unit cell parameters	
a	13.851(1) Å
b	16.798(1) Å
c	5.1581(4) Å
V	1200.1(2) Å³
Z	4
D_{calc} (g.cm⁻³)	3.65
μ (mm⁻¹)	11.22
Refinement by Jana2006	
Profile function; correction for asymmetry	Pseudovoigt, Simpson
No. observed diffractions [$I > 3\sigma(I)$]	140
No. profile parameters	19
No. structural parameters	35
R_p	0.1357
R_{wp}	0.1859
R_F	0.0733
GOF	2.11
R_{Bragg}	0.1392
$\Delta\rho_{max}$, $\Delta\rho_{min}$ (e Å⁻³)	−0.85, 0.91

Indices of agreement defined according to McCusker et al. (1999) and Petříček et al. (2006)

standard setting *Bbmm* of the space group *Cmcm* was used. Background was approximated using Legendre polynomials of the 12th order. A Pseudovoigt profile function was selected to describe peak-shape of reflections corrected for asymmetry (Simpson model). The unit-cell parameters, shift (zero-error) and halfwidth parameters were refined in the first cycles of the refinement. The refinement procedure converges quickly to the global $R_p \sim 14\%$. Estimated standard uncertainties were corrected for local correlations after the procedure of Bérar and Lelann (1991). Details for the data collection and refinement are listed in Tab. 4. The structure was plotted by the DIAMOND program (Crystal Impact; Brandenburg and Putz 2005). For some additional, namely geometrical parameters, the VESTA software (Momma and Izumi 2008) was utilized. The bond-valence calculations are based on the bond-valence parameters given by Brown and Altermatt (1985).

Tab. 5 Atomic co-ordinates, displacement parameters, site-occupancies and numbers of atoms (*apfu*) for crystal structure of plimerite from Krásno

	Site	x	y	z	U_{iso} [Å²]	M/Z	SOF	apfu
M1 (Fe^{3+})	4*a*	0	0.5	0	0.04(1)	1	1.00(6)	1
M2 (Zn,Fe)	8*f*	0.067(1)	0.6577(8)	0.00	0.045(5)	2	0.6, 0.4*	1.20, 0.80
M3 (Fe^{3+})	16*h*	0.322(1)	0.640(1)	0.229(4)	0.019(1)	4	0.58(2)	2.32
P1	8*f*	0.141(2)	0.545(2)	0.50	0.02(1)	2		2
P2	4*c*	0.487(3)	0.75	0.00	0.03(1)	1		1
O1	8*g*	0.554(3)	0.75	−0.23(1)	0.01(2)	2		2
O2	16*h*	0.083(2)	0.557(2)	0.264(8)	0.00(3)	4		4
O3 (OH)	8*g*	0.315(6)	0.75	0.38(1)	0.0143	2	0.5	1
O4	8*f*	0.176(4)	0.462(4)	0.50	0.05(2)	2		2
O5 (OH)	8*f*	0.218(4)	0.674(3)	0.00	0.02	2		2
O6 (OH)	8*f*	0.077(5)	0.391(3)	0.00	0.014	2		2
O7	8*f*	0.417(4)	0.673(3)	0.00	0.016	2		2
O8	8*f*	0.222(4)	0.609(3)	0.50	0.02(2)	2		2

M/Z – site multiplicity/formula units (for Z = 4); SOF – structure occupancy factors (derived from the refinement); *apfu* – resulting atoms per formula unit; * occupancies derived from EPMA

5.2. Results

The crystal structure refinement of plimerite from Krásno based on high-resolution synchrotron powder diffraction data (Fig. 16) confirmed basically the structure reported by Elliott et al. (2009) despite of few differences. As the composition of the plimerite sample, obtained by EPMA study, differs from that of Elliott et al. (2009), elements entering the sites and corresponding site-occupancies were refined. Chiefly, the main differences between these two structure refinements consist in the site-occupancies derived from the corresponding site-symmetries.

The atomic coordinates and isotropic displacement parameters are listed in Tab. 5, selected interatomic distances and geometrical parameters in Tab. 6. Current crystal structure refinement confirmed the three cation sites present in the crystal structure of plimerite that we designated in accordance with Elliot et al. (2009) as $M1$, $M2$ and $M3$ positions (Fig. 17). All the three exhibit distorted octahedral coordination. Here, as results of the refinement and bond-valence analysis suggests (Tabs 6–7), $M1$ and $M3$ positions are solely occupied by trivalent cations, in our case by Fe^{3+}. We introduced into the refinement Al^{3+} into $M3$ position, however it turned out negative values of atomic occupation factor same as unrealistic low bond-valence sums for Al^{3+} (~ 2.2 *v.u.*). The trials to run the refinement with Al^{3+} were therefore abandoned and these two positions were considered to be occupied solely by Fe^{3+}. Our assignment of the Fe atoms as trivalent is consistent with the sums obtained from the bond-valence analysis (Tab. 7). The refined occupancies for these sites are 1.00(6) and 0.58(2) for $M1$ and $M3$, respectively. The occupancy of $M3$ site is somewhat higher than expected from EPMA results. However, the refinement converged quite quickly to these values and attempts to run the refinement with constrained occupancies led to a significantly worse fit. The $M2$ position was found to be occupied by divalent cations; it is apparent from the interatomic distances obtained from the refinement (Tab. 6). The $M2$ site exhibits considerable distortion from the ideal octahedral symmetry (Tab. 6), as consistent with the structural refinement by Redhammer et al. (2006). In accordance to Elliot et al. (2009) we introduced into the structural model Zn^{2+} besides Fe^{2+} in the $M2$ position. However, the refinement of the site-occupancy was not successful; the R factors were considerably worse and the difference curve showed considerable disagreement between calculated and observed profiles. Therefore we set the fix values based on the results of electron microprobe (0.6 for Zn, that means $0.6 \times 2 = 1.2$ Zn *apfu*, 0.4 for Fe, $0.4 \times 2 = 0.8$ Fe *apfu*; the full site occupancy = 1).

Tab. 6 Selected interatomic distances (Å) and geometrical parameters for refined structure of Krásno plimerite

M1		M2	
Fe1–O2 (4×)	2.02(4)	$M2$–O1 (2×)	2.09(4)
Fe1–O6 (2×)	2.11(5)	$M2$–O2 (2×)	2.17(4)
<Fe1–O>	2.05	$M2$–O5	2.09(5)
V_{M1}	11.21	$M2$–O6	2.14(6)
Δ	0.0183	<$M2$–O>	2.12
σ^2	57.64	V_{M2}	12.36
EcoN	5.92	Δ	0.0175
		σ^2	83.30
		EcoN	5.93
M3		P1–O2 (2×)	1.47(4)
$M3$–O3	2.00(5)	P1–O4	1.47(7)
$M3$–O4	2.08(3)	P1–O8	1.55(6)
$M3$–O5	1.96(5)	<P1–O>	1.49
$M3$–O6	2.06(5)	Δ	0.0197
$M3$–O7	1.86(5)	σ^2	8.48
$M3$–O8	2.05(5)	EcoN	3.93
<$M3$–O>	2.00	P2–O1 (2×)	1.44(6)
V_{M3}	10.58	P2–O7 (2×)	1.61(6)
Δ	0.0307	<P2–O>	1.53
σ^2	28.97	Δ	0.0540
ECoN	5.56	σ^2	7.80
		EcoN	3.51
O1–O1^{iv}	2.75(7)	O3–O6^{x}	2.87(7)
O1–O1^{vi}	2.41(7)	O3–O7^{ix}	2.75(8)
O1–O7	2.49(6)	O3–O7^{x}	2.75(8)
O2–O2^{i}	2.99(5)	O3–O8	2.75(7)
O2–O2^{iii}	2.72(5)	O3–O8^{vi}	2.75(7)
O2–O2^{v}	2.44(5)	O4–O5^{xi}	2.71(8)
O2–O4	2.39(6)	O4–O7^{i}	2.60(8)
O2–O6	2.75(6)	O4–O8	2.57(8)
O2–O8	2.44(6)	O5–O5^{iv}	2.56(7)
O3–O3^{vi}	1.23(10)	O5–O7^{ix}	2.76(8)
O3–O5	2.70(8)	O5–O8	2.80(3)
O3–O5^{iv}	2.70(8)	O5–O8^{xii}	2.80(3)
O2–O10	2.843(19)	O6–O7	2.80(3)
O3–O3^{v}	2.37(3)	O6–O7^{xii}	2.80(3)
O3–O5	2.70(8)	O6–O8^{xiii}	2.78(8)
O3–O5^{vi}	2.70(8)	O7–O7^{vi}	2.58(7)
O3–O6^{viii}	2.87(7)		

Symmetry codes: (i) −x, −y+1, z; (ii) −x, −y+1, −z; (iii) x, y, −z+1; (iv) x, −y+3/2, −z; (v) x, y, −z+1; (vi) x, −y+3/2, −z+1; (vii) −x+1/2, −y+1, z−1/2; (viii) x+1/2, y, z+1/2; (ix) x+1/2, y, z−1/2; (x) x+1/2, −y+3/2, −z+1/2; (xi) −x+1/2, −y+1, z+1/2; (xii) x, y, z−1; (xiii) x−1/2, y, z−1/2.

Δ, bond-length distortion after Brown and Shannon (1973); σ^2, bond-angle distortion (variance) after Robinson et al. (1971); ECoN, an effective coordination number after Hoppe (1979).

From the structure refinement the sum of the cations is therefore $Zn_{1.2}(Fe^{2+} + Fe^{3+})_{4.12}$.

There are two symmetrically independent P atoms in the structure of plimerite, both forming $(PO_4)^{3-}$ tetrahedra. Bond-valence sums for both atoms obtained from bond-valence analysis are consistent with the assignment as
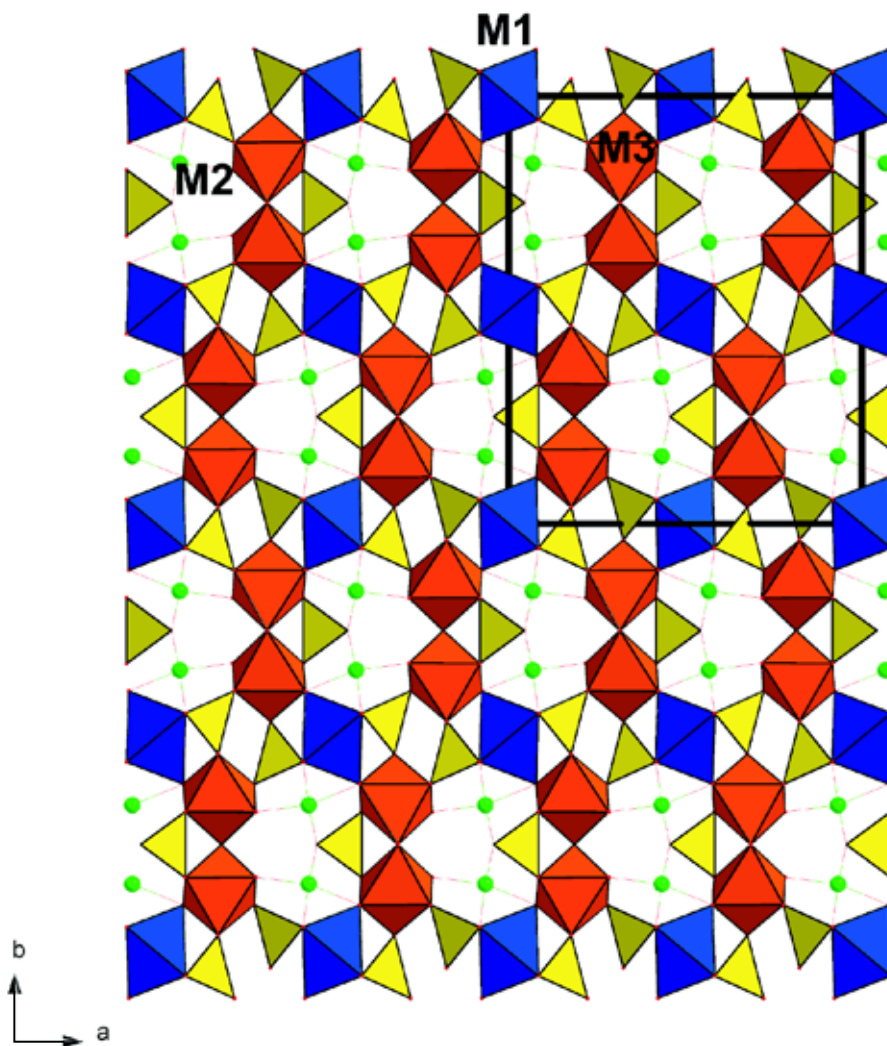
Fig. 17 The crystal structure of plimerite from Krásno in the projection along [001] direction. *M1* represents Fe^{3+} position (blue octahedra), *M2* the site containing divalent cations (green) and *M3* the Fe^{3+} position (orange); phosphate tetrahedra are yellow. Unit-cell edges are outlined by the solid bold line.

P^{5+}. However, the sum for P1 atom is somewhat higher than expected from the formal oxidation state.

Based on bond-valence analysis for the plimerite refined structure, the assignment of the further anionic species may be done. As suggest obtained sums (Tab. 7), O3, O5 and O6 atoms may be designated as OH$^-$ groups.

Obviously, the atoms O4, O7 and O8 are somewhat undersaturated (see Tab. 7), and this may suggest that these anions represent mixture of O^{2-}/OH$^-$ or O^{2-}/H$_2$O. The O3 atom is localized at shared apex of the FeO$_6$ octahedra (Fig. 18). The O3 site is situated ~ 0.6 Å from the mirror plane, which results in a separation of O3–O3 sites of

Tab. 7 Bond-valence analysis for the refined crystal structure of Krásno plimerite

	M1	Fe2	Zn2	M3	P1	P2	∑BV	Assign.
O1		0.40 ×2↓	0.34 ×2↓			1.61 ×2↓	1.98	O^{2-}
O2	0.49 ×4↓	0.32 ×2↓	0.28 ×2↓		1.49 ×2↓		2.28	O^{2-}
O3				0.52 ×2→			1.04	OH$^-$
O4				0.42	1.45		1.87	O^{2-}
O5		0.40	0.34	0.60			0.97	OH$^-$
O6	0.38 ×2↓	0.33	0.28	0.46			0.95	OH$^-$
O7				0.77		1.02 ×2↓	1.79	O^{2-}
O8				0.48	1.14		1.62	O^{2-}
∑BV	2.72	2.17	1.86	3.25	5.57	5.26		

Values are expressed in valence units (*v.u.*). Multiplicity is indicated by × 2↓; all bond strengths were taken from Brown and Altermatt (1985); Zn^{2+}/Fe^{2+} site occupancy (0.6/0.4) used in calculations
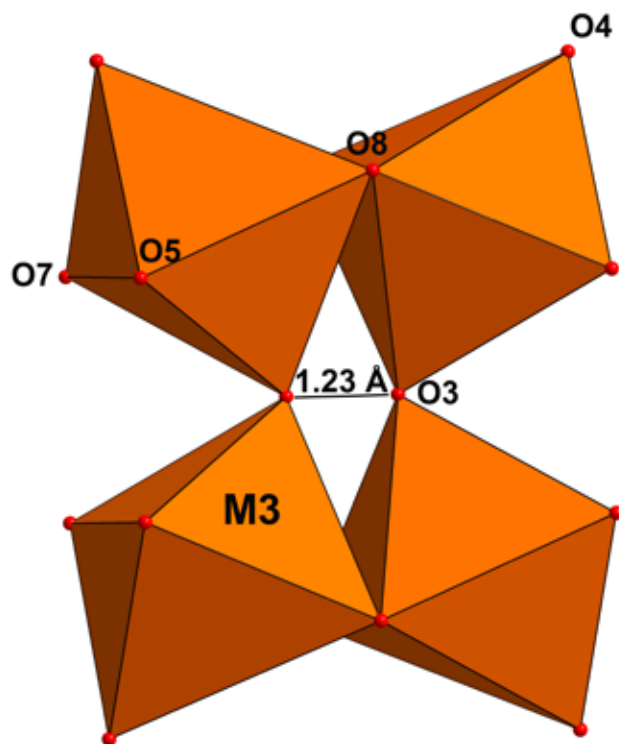
Fig. 18 Sharing of *M3* octahedra projected in a general direction.

1.23 Å. Thus, these sites are not fully occupied, showing occupancy of ~ 0.5. This is consistent with the results of Moore (1970) and Redhammer et al. (2006) for rockbridgeite as well as of Elliot et al. (2009) for plimerite.

Hence, the formula of studied plimerite is different from the generally accepted frondelite–rockbridgeite formula $A^{2+}B^{3+}_4(TO_4)_3(OH)_5$ (Redhammer et al. 2006; Elliot et al. 2009). Based on the results of the crystal structure refinement and bond-valence analysis, the formula of Krásno plimerite is more likely $(Zn_{1.20}Fe_{0.80})_{\Sigma 2.00}Fe_{3.32}(PO_4)_{3.00}(OH)_{5.00}$, Z = 4. This formula is not electro neutral; however, as there is 0.04− excess which is considered negligible and more likely than the difference reported by Elliot et al. (2009) of 0.63−. This small excess is probably within the error of the structure refinement (site-occupancies) and may be compensated by above-mentioned mixtures of the anionic species.

There is no direct indication of the presence of molecular H_2O in the structure of plimerite from the structure refinement, except only the above-mentioned possibility of OH^-/H_2O disorder. Analysing interatomic distances, just two less probable configurations may play a role. One is a cavity defined by O4–O4 (3.54 Å) and O8–O8 (4.56 Å) separations. The second is space with the size defined by O1–O3 (3.80 Å) and O5–O5 (2.56 Å) separations. A weakly bonded molecular H_2O, which may be designated as zeolitic, perhaps occupies these two cavities.

6. Discussion

Five morphologically different types of the mineral plimerite were identified in the samples from the Huber open pit, the Krásno ore district (Czech Republic) by EPMA and PXRD. Detailed mineralogical data, including IR and Raman spectroscopy, were obtained for plimerite type 1.

The crystal structure of the studied plimerite generation was refined by the Rietveld method from the high-resolution synchrotron powder diffraction data. The formula of studied plimerite from Krásno obtained from the crystal structure refinement and bond-valence analysis is $(Zn_{1.20}Fe_{0.80})_{\Sigma 2.00}Fe^{3+}_{3.32}(PO_4)_{3.00}(OH)_{5.00}$. This is inconsistent with the formula presented previously by Elliot et al. (2009) from the structural refinement of plimerite from Australia (G32401), which was considerably non-electro neutral.

The ideal formula of plimerite probably should not be expressed as $ZnFe^{3+}_4(PO_4)_3(OH)_5$, as suggested Elliot et al. (2009). Inspecting their derived structural formulae for two samples, $Zn_{1.41}Fe^{2+}_{0.30}Fe^{3+}_{2.71}Al_{0.58}(PO_4)_3(OH)_5$ (sample G32005) and $Zn_{1.17}Fe^{2+}_{0.37}Fe^{3+}_{3.46}(PO_4)_3(OH)_5$ (G32401), the disharmony with their derived ideal formula is obvious, and they did not discuss these discrepancies any further. According to the structural analysis of Redhammer et al. (2006) on Mn-rich rockbridgeite, the chemical composition of ions in the *M2* position may be expressed as $Fe_{1.32}Mn_{0.62}Zn_{0.06}$, based on structural refinement and electron microprobe analyses. The structural formula obtained by Redhammer et al. (2006) from the refinement is $Fe_{4.32}Mn_{0.62}Zn_{0.06}(PO_4)_3(OH)_5$. According to the refinement and Mössbauer spectroscopy, the position Fe1 site (*M1*) is filled with 0.98 (3) Fe^{3+} *apfu*, while the Fe3 site (*M3*) should contain 2.00 (3) Fe^{3+} *apfu*. The problem remaining in the paper of Redhammer et al. (2006) is the valence state of Mn. The authors assigned it finally as Mn^{3+}, because it yielded a more homogeneous formula than calculation with divalent Mn. Therefore they presented a formula $Ca_{0.05}Na_{0.06}Zn_{0.06}Mn^{3+}_{0.61}Fe^{2+}_{1.22}Fe^{3+}_{3.14}(P_{3.01}O_{12})(OH)_5$ for the Mn-rich rockbridgeite, where Ca and Na probably reside in the interstices. It may be concluded both from the current refinement and that by Elliot et al. (2009) that some degree of disorder on the *M1/M2/M3* sites might occur in these structures. Currently presented refined structure should be interpreted in the view as a model, considering the differences between the formula obtained from the microprobe study and structural refinement. This model assumes that M^{2+}/M^{3+} cations sit in different sites; however, it is quite probable that they are partly distributed over each *M1/M2/M3* site in the crystal structure.

Presence of molecular H_2O deduced from the TG analysis and IR/Raman spectroscopy is not supported by the results of the crystal structure refinement. However, the crystal structure is probably able to accommodate

"zeolitic water" – only weakly bonded H_2O in the small cavities in the structure, plus a probable disorder involving some of the O sites in the structure of plimerite. We do not suppose presence of more than one H_2O molecule. No significant structural changes were observed at elevated temperatures by the high-resolution synchrotron diffraction study up to ~ 280–300 °C (personal communication by J. Plášil).

References

Beran P, Sejkora J (2006) The Krásno Sn–W ore district near Horní Slavkov: mining history, geological and mineralogical characteristics. J Czech Geol Soc 51: 3–42

Bérar J-F, Lelann P (1991) E.s.d.'s and estimated probable errors obtained in Rietveld refinements with local correlations. J Appl Cryst 24: 1–5

Birch WD (1990) Minerals from the Kintore and Block 14 Opencuts, Broken Hill, N.S.W.: a review of recent discoveries, including tsumebite, kipushite and otavite. Austral Miner 5: 125–141

Brandenburg K, Putz H (2005) DIAMOND Version 3. Crystal Impact GbR, Postfach 1251, D-53002 Bonn, Germany

Brown ID, Altermatt D (1985) Bond-valence parameters obtained from a systematic analysis of the inorganic crystal structure database. Acta Cryst B41: 244–248

Brown ID, Shannon RD (1973) Empirical bond-strength bond-length curves for oxides. Acta Cryst A29: 266–282

Elliott P, Kolitsch U, Giester G, Libowitzky E, McCammon C, Pring A, Birch WD, Brugger J (2009) Description and crystal structure of a new mineral – plimerite,

$ZnFe_4^{3+}(PO_4)_3(OH)_5$ – the Zn-analogue of rockbridgeite and frondelite, from Broken Hill, New South Wales, Australia. Mineral Mag 73: 131–148

Ginzburg AI (1952) The phosphates of granite pegmatites. Trudy Mineral Muz Akad Nauk SSSR 4: 36–63

Hirson JR (1965) Note sobre os fosfatos de Sapucai. Anais Acad Brasil Cien 37: 471–475

Hoppe R (1979) Effective coordination numbers (ECoN) and mean fictive ionic radii (MEFIR). Z Kristallogr 150: 23–52

Johnson JE (1978) Zinc phosphate minerals from Reaphook Hill, South Australia. Austral Miner 1: 65–68

Lindberg ML, Frondel C (1950) Zincian rockbridgeite. Amer Miner 35: 1028–1034

McCusker LB, Von Dreele RB, Cox DE, Louër D, Scardi P (1999) Rietveld refinement guidelines. J Appl Cryst 32: 36–50

Mills SJ, Kolitch U, Birch WD, Sejkora J (2008) Kunatite, $CuFe_2(PO_4)_2(OH)_2 .4H_2O$, a new member of the whitmoreite group, from Lake Boga, Victoria, Australia. Austr J Miner 14: 3–12

Momma K, Izumi F (2008) VESTA: a three-dimensional visualization system for electronic and structural analysis. J Appl Cryst 41: 653–658

Moore PB (1970) Crystal chemistry of basic iron phosphates. Amer Miner 55: 135–169

Petříček V, Dušek M, Palatinus L (2006) Jana2006. The crystallographic computing system. Institute of Physics, Academy of Sciences, Prague, *http://jana.fzu.cz/*

Pouchou JL, Pichoir F (1985) "PAP" ($\varphi\rho Z$) procedure for improved quantitative microanalysis. In: Armstrong JT (ed) Microbeam Analysis. San Francisco Press, San Francisco, pp 104–106

Redhammer GJ, Roth G, Tippelt G, Bernroider M, Lottermoser W, Amthauer G, Hochleitner R (2006) Manganoan rockbridgeite $Fe_{4.32}Mn_{0.62}Zn_{0.06}(PO_4)_3(OH)_5$: structure analysis and ^{57}Fe Mössbauer spectroscopy. Acta Cryst C62: i24–i28

Robinson K, Gibbs GV, Ribbe PH (1971) Quadratic elongation: a quantitative measure of distortion in coordination polyhedra. Science 172: 567–570

Sejkora J, Ondruš P, Fikar M, Veselovský F, Mach Z, Gabašová A, Škoda R, Beran P (2006a) Supergene minerals at the Huber stock and Schnöd stock deposits, Krásno ore district, the Slavkovský les area, Czech Republic. J Czech Geol Soc 51: 57–101

Sejkora J, Škoda R, Ondruš P (2006b) New naturally occurring mineral phases from the Krásno–Horní Slavkov area, western Bohemia, Czech Republic. J Czech Geol Soc 51: 159–187

Sejkora J, Škoda R, Ondruš P, Beran P, Süsser C (2006c) Mineralogy of phosphate accumulations in the Huber stock, Krásno ore district, Slavkovský les area, Czech Republic. J Czech Geol Soc 51: 103–147